ARTICLES
PUBLISHED ONLINE: 20 JUNE 2010 | DOI: 10.1038/NCHEM.695
nature chemistry

Lewis acid-catalysed formation of two-dimensional phthalocyanine covalent organic frameworks

Eric L. Spitler and William R. Dichtel*

Covalent organic frameworks (COFs) offer a new strategy for assembling organic semiconductors into robust networks with atomic precision and long-range order. General methods for COF synthesis will allow complex building blocks to be incorporated into these emerging materials. Here we report a new Lewis acid-catalysed protocol to form boronate esters directly from protected catechols and arylboronic acids. This transformation also provides crystalline boronate ester-linked COFs from protected polyfunctional catechols and bis(boronic acids). Using this method, we prepared a new COF that features a square lattice composed of phthalocyanine macrocycles joined by phenylene bis(boronic acid) linkers. The phthalocyanines stack in an eclipsed fashion within the COF to form 2.3 nm pores that run parallel to the stacked chromophores. The material's broad absorbance over the solar spectrum, potential for efficient charge transport through the stacked phthalocyanines, good thermal stability and the modular nature of COF synthesis, show strong promise for applications in organic photovoltaic devices.

The continuing development of organic semiconductors[1] will bring about flexible displays[2], radiofrequency identification tags[3], improved lighting technologies[4], efficient sensors[5,6] and economically competitive solar cells[7,8]. In addition to their low cost, one of the most attractive aspects of organic electronic materials is the promise of tuning the properties of a device through rational chemical design and synthesis. Known structure–property relationships and computational tools enable predictable tuning of the bandgaps and frontier molecular orbital energies of organic semiconductors. However, control of the packing and long-range order is also critical for efficient charge transport through the material[9]. Efforts in crystal engineering produced examples of cofacially packed pentacene[10] and tetrathiafulvalene[11] derivatives, but to predict the crystal structures of small organic molecules reliably remains an unsolved challenge[12]. Varying the identity or positions of substituents to tune electronic properties can induce unpredictable changes in long-range order, which limits the generality of molecular design strategies.

COFs comprise an emerging class of materials that can overcome these challenges[13–15]. COFs incorporate organic subunits into periodic two-dimensional (2D) and three-dimensional porous crystalline structures held together by covalent bonds rather than by non-covalent interactions. These linkages provide robust materials with precise and predictable control over composition, topology and porosity, features first exploited for gas-storage applications[16]. The relative geometries of the reactive groups in the starting materials determine the COF's topology, which does not change significantly as other functional groups are varied. 2D COFs predictably assemble functional aromatic systems into cofacially stacked morphologies ideal for transporting excitons or charge carriers through the material[17,18]. Although COFs linked by boroxines[13,18], imines[19] and borosilicates[20] are reported, the most widely studied COFs are linked by boronate ester moieties[14,21]. The boronate ester-linked materials are particularly promising for organic electronics, in part because they incorporate two distinct molecular components that allow their composition and porosity to be varied independently.

Despite their great promise, the limited generality of synthetic methods for COFs represents a significant barrier to realizing their potential fully. Since they were first reported in 2005, all boronate ester-linked COFs have been synthesized through the solvothermal condensation of polyfunctional boronic acids and catechols. However, only 2,3,6,7,10,11-hexahydroxytriphenylene (HHTP) and four 1,2,4,5-tetrahydroxybenzene derivatives have produced crystalline materials, and HHTP is the only building block used more than once. Reports of new boronate ester-linked COFs ceased after an initial flurry of activity. This lack of progress is attributable to undesirable features of compounds that contain multiple catechol moieties. Polyfunctional catechols are prone to oxidation and are often sparingly soluble in organic solvents, factors that hinder both the preparation of useful quantities of functionalized monomers and their incorporation into COFs.

Here we report a new general method for the synthesis of boronate ester-linked COFs that avoids the direct use of insoluble and unstable polyfunctional catechol reactants. Using this method we prepared a 2D network of cofacially stacked phthalocyanines, chromophores that absorb strongly and have been employed in both bulk heterojunction[22,23] and dye-sensitized solar cells[24], as well as in many other applications[25–27]. The phthalocyanine COF forms an eclipsed 2D square lattice as determined by powder X-ray diffraction (PXRD), surface area analysis and ultraviolet–visible, near infrared and fluorescence spectroscopies. This material represents a key first step towards forming COF-based bulk heterojunctions that feature structurally precise and large surface area interfaces between complementary organic semiconductors.

Results and discussion

The direct formation of boronate esters from protected catechols presents an attractive alternative for COF synthesis because the protecting groups can decrease the compound's polarity, prevent autoxidation and confer enhanced solubility. Although we are aware of only a single example of a related transformation[28], we found (Fig. 1) that phenylboronic acid **1** reacts cleanly with catechol acetonide **2** to form the corresponding catechol boronate ester **3** in the presence of substoichiometric amounts of the Lewis acid $BF_3{\cdot}OEt_2$. The reaction takes place over the course of a few hours at

Department of Chemistry and Chemical Biology, Cornell University, Baker Laboratory, Ithaca, New York 14853-1301, USA. *e-mail: wdichtel@cornell.edu

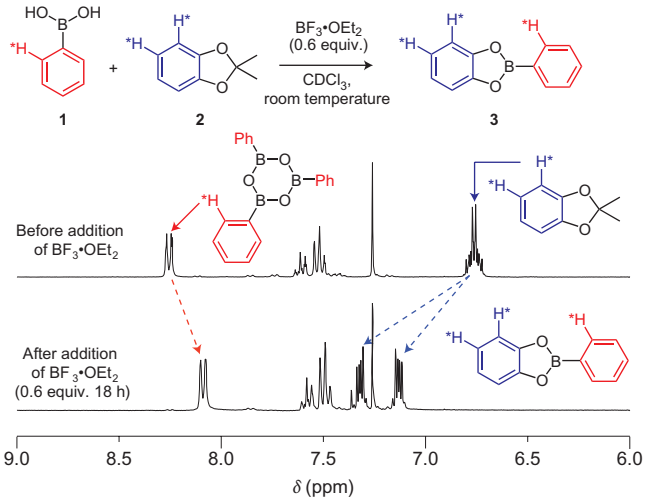

Figure 1 | BF_3·OEt_2 catalyses the formation of 2-phenyl-1,3,2-benzodioxaborole (3) from phenylboronic acid (1) and catechol acetonide (2). The partial ^{1}H NMR spectra (300 MHz, 298 K, $CDCl_3$) of the reaction mixture before and 18 hours after the addition of BF_3·OEt_2 showed a clean conversion of **1** (which rapidly dehydrates to the corresponding boroxine when dissolved in $CDCl_3$) and **2** to the corresponding boronate ester **3**. No resonances that correspond to free catechol were observed in spectra taken at intermediate conversion.

millimolar concentrations of starting materials in several ether and non-coordinating solvents at mild temperatures (20–85 °C), and does not require the rigorous exclusion of oxygen or water. We next confirmed that this transformation can produce crystalline COFs by synthesizing COF-5 and COF-10, previously reported by Yaghi and co-workers[13,29], through the condensation of HHTP tris(acetonide) and the appropriate bis(boronic acid). Spectral data of the materials obtained under Lewis acid-catalysed conditions matched those reported previously (see Supplementary Fig. S22).

The phthalocyanine tetra(acetonide) **4** (Fig. 2) is a suitable equivalent tetrafunctional catechol for the formation of COFs under the above BF_3·OEt_2-catalysed boronate esterification conditions. Multigram quantities of **4** were obtained by modifying a synthetic procedure reported by Breslow and co-workers[30]. Phthalocyanine **4** is moderately soluble in many organic solvents and stable under ambient conditions. In contrast, the corresponding octahydroxyphthalocyanine was reported as a highly insoluble solid that must be stored under an inert atmosphere to prevent its oxidation[31,32]. **Pc-PBBA COF** was synthesized by combining **4** (**Pc**) (32 mg), 1,4-phenylenebis(boronic acid) (**PBBA**) (**5**, 18.5 mg) and BF_3·OEt_2 (0.015 ml) in a 1:1 mixture of mesitylene and 1,2-dichloroethane (DCE) in a flame-sealed glass reaction vessel. The sealed tube was placed in a 120 °C oven for six days. The resulting green precipitate was collected by filtration and washed with anhydrous MeCN to isolate **Pc-PBBA COF** in 48% yield. The isolated COF displayed excellent thermal stability to 500 °C, as determined by thermogravimetric analysis.

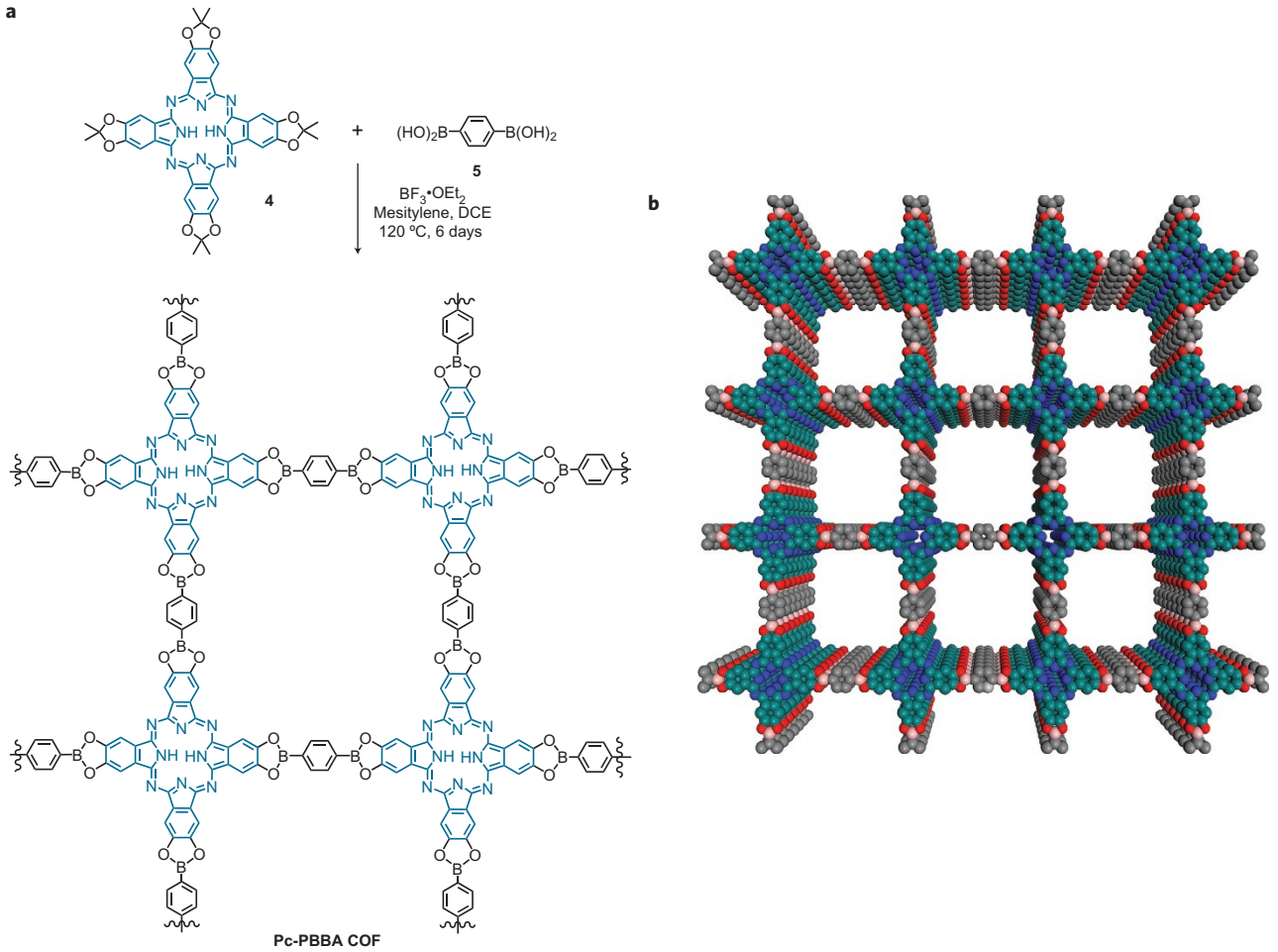

Figure 2 | Lewis acid-catalysed boronate ester formation conditions provide an eclipsed 2D COF that consists of phthalocyanines linked by PBBA. a, The Lewis acid-catalysed deprotection–condensation protocol was used to form the **Pc-PBBA COF** from phthalocyanine tetra(acetonide) **4** and PBBA **5**. **b**, **Pc-PBBA COF** exhibits a square lattice with 2D sheets that form eclipsed stacks.

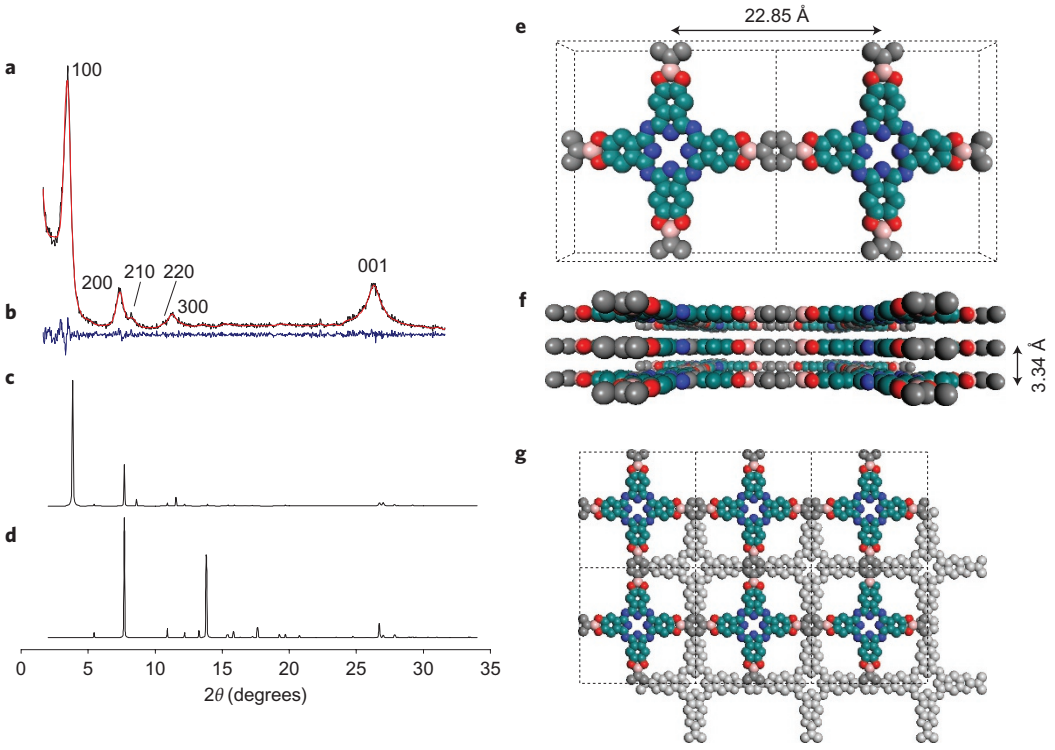

Figure 3 | X-ray diffraction confirms that the Pc-PBBA COF is a crystalline material with an eclipsed 2D structure. a, The experimental PXRD pattern (black; the major observed reflections are labelled) and Pawley refined (red) pattern of **Pc-PBBA COF. b**, A difference plot between the experimental and refined diffraction patterns shows excellent agreement. **c**, A simulated PXRD pattern for a **Pc-PBBA COF** square lattice shows good agreement with the experimental and refined patterns. **d**, A simulated PXRD for a theoretical 2D staggered structure (**g**) does not agree with the experimental and refined patterns. **e**,**f**, The crystal parameters extracted from the Pawley-refined PXRD are displayed on a model of the **Pc-PBBA** lattice. **g**, Theoretical 2D staggered structure.

The PXRD pattern of **Pc-PBBA COF** (Fig. 3a, black) indicated that it is a crystalline material consistent with the long-range structure depicted in Fig. 2. The most intense peak at $2\theta = 3.84^\circ$ corresponds to the (100) and (010) diffractions of the square lattice. The minor diffraction peaks at 7.68°, 8.52°, 11.56° and 26.64° correspond to the (200), (210), (300) and (001) diffractions, respectively. None of the observed peaks correspond to the phthalocyanine or the acid starting materials (see Supplementary Fig. S9). Pawley refinement of the observed PXRD pattern profile using the Reflex Plus module of the Materials Studio version 4.4 suite of programs[33] (Fig. 3a, red) produced the unit-cell parameters $a = b = 22.85$ Å and $c = 3.34$ Å (Fig. 3e,f) and confirmed the assignment of the observed reflections. The refined profile matches the observed powder diffraction pattern very well, with profile-fitting factors that converge to a weighted *R*-factor (wR_p) of 9.72% and R_p of 6.46%. The difference plot (Fig. 3b) also indicates a good fit in which the only deviations appear in the very low angle region, where background interference is greatest.

Simulation of the PXRD pattern of the eclipsed 2D **Pc-PBBA** lattice (Fig. 3c) showed good agreement with the experimental data. We constructed a unit-cell precursor that consisted of a phthalocyanine macrocycle functionalized with phenylboronate esters at each of the four termini (Fig. 3e) and optimized its geometry (hydrogen atoms were omitted). A tetragonal crystal of D_{4h} ($P4/mmm$) symmetry was then generated with initial lattice parameters *a* and *b* that corresponded to the distance between the centroids of phenylene units on opposite sides of the cell (about 23 Å). Initially, the interlayer spacing *c* was set at 3.33 Å, the π–π stacking distance in boron nitride[34]. The crystal geometry was reoptimized, and the resulting simulated powder diffraction pattern matched the experimental peak positions and intensities quite well. The calculated lattice parameters ($a = b = 22.96$ Å, $c = 3.34$ Å) from this model were also quite close to the measured and refined parameters ($a = b = 22.85$ Å, $c = 3.34$ Å).

We also considered an alternative staggered 2D arrangement (Fig. 3g) in which the phthalocyanine units of adjacent sheets are horizontally offset by a distance of $a/2$ and $b/2$. The simulated PXRD pattern for this arrangement (Fig. 3d) does not match the experimental data. We attribute the formation of the eclipsed structure to the strong tendency for phthalocyanine units to form cofacial aggregates that are reinforced by stabilizing B–O interactions between adjacent layers.

Two distinct crystal morphologies were observed by scanning electron microscopy imaging of **Pc-PBBA COF**, one with a striated rectangular prism shape that averaged approximately 1 μm in length and 200–300 nm in thickness and one of flattened irregular plates 2–4 μm long (Fig. 4). The presence of these two phases may account for line broadening in the PXRD pattern, and could be the result of different nucleation or growth environments in the reaction vessel.

The Fourier transform infrared (FTIR) spectrum of **Pc-PBBA COF** obtained in attenuated total reflectance (ATR) mode indicated the formation of boronate ester rings through the strong B–O stretch at 1,328 cm^{-1} (see Supplementary Fig. S3). An analogous band at 1,344 cm^{-1} appeared in the spectrum of **5**, although the two spectra were otherwise quite different. The hydroxyl bands of the COF were attenuated greatly relative to the starting materials, consistent with free hydroxyl groups at the edges of the crystallites or at defects. The phthalocyanine acetonide **4** shared many infrared absorbances with the **Pc-PBBA COF** material, although the methyl C–H stretches from the acetonide-protecting groups were notably absent from the COF spectrum. Also, we obtained an

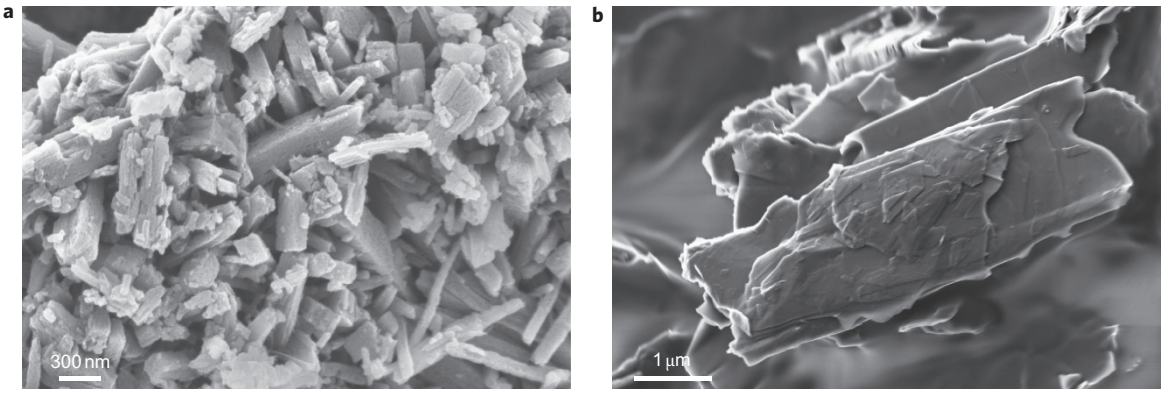

Figure 4 | Scanning electron micrographs of the Pc-PBBA COF display two crystal morphologies. a,**b**, These include (**a**) rectangular prisms about 1 μm in length and (**b**) flat sheets of 2–4 μm long.

FTIR spectrum of a crude sample of octahydroxyphthalocyanine (produced by treating **4** with $BF_3{\cdot}OEt_2$ in the absence of **5**). Its FTIR spectrum is distinct from that of the COF (see Supplementary Fig. S4). These observations provide strong evidence for the formation of the boronate ester-linked material.

The porosity and surface area of the material was measured by nitrogen-gas adsorption. An adsorption isotherm between 0 and 1 atmosphere was generated after evacuation under continuous vacuum for 12 hours at 180 °C (Fig. 5). We observed a sharp initial uptake at low pressures as the small pores filled, followed by a more gradual uptake over the remainder of the pressure range. Desorption occurred with a small hysteresis at about $P/P_0 = 0.5$ ($P_0 = 1$ atm). The Langmuir surface-area model was applied to the $P/P_0 = 0.02$–0.06 (16–43 mm Hg) region of the isotherm, where the initial adsorption was most linear. The calculated Langmuir surface area from these data was 506 $m^2\ g^{-1}$, which is slightly low relative to other reported COFs, but still well within the values of other micro- and mesoporous materials, such as zeolites and several metal–organic frameworks[35–40]. The increased density of a square lattice combined with the relatively small phenylene linker unit results in a material of lower surface area. This trend has been observed in series of COFs with gradually increasing pore size[26,27].

The Barrett–Joyner–Halenda (BJH) adsorption–desorption model was used to study the pore size and volume distributions (see Supplementary Fig. S15)[41,42]. Pore-distribution plots revealed a maximum pore area of 469 $m^2\ g^{-1}$ at a width of 2.12 nm and a maximum pore volume of 0.258 $cm^3\ g^{-1}$ at a width of 2.17 nm. Peaks at larger pore sizes likely result from uptake in structural defects or slipped sheets along the micropore walls. The BJH model is most appropriate for mesoporous materials with pore sizes between 2 and 300 nm. **Pc-PBBA COF** has a predicted pore width of approximately 2 nm, which is at the lower limit. Even with this limitation, the pore data match predictions from the Materials Studio program reasonably well.

Phthalocyanines strongly absorb visible light and are thus deep blue or green compounds, depending on the identity (or absence) of a metal ion coordinated to the four central nitrogen atoms. The electronic absorption spectra of dilute CH_2Cl_2 solutions of **3** ($\sim 10^{-6}$ M) are typical of non-aggregated, free-base phthalocyanines. The sharp peaks at 653 and 691 nm located within the broad absorption band from 500 to 725 nm (*Q* band) are hallmarks of monomeric phthalocyanine macrocycles. Diffuse reflectance spectra (Fig. 6) obtained from powders of both **Pc-PBBA COF** and **4** showed a blue shift of these maxima (11 nm for the COF and 66 nm for **4**, respectively) consistent with the formation of cofacially stacked H-aggregates, as well as broadening of the *Q* band into the near infrared. Similar blue shifts and spectral band broadening were observed for solutions of aggregated phthalocyanines and in liquid crystalline phases of cofacially aligned phthalocyanine discotic mesogens[43]. The COF spectrum is red-shifted from that of **4** by a small amount, which probably arises from differences in aggregation geometry as well as the electron-withdrawing nature of the boronate esters relative to the acetonide functionalities. The changes in absorbance properties exhibited by **Pc-PBBA COF**, particularly the broadening of the absorbance to enhance absorption in the 450–600 nm region and the tailing into the near infrared, make these materials promising candidates for the collection of solar energy.

Photoluminescence measurements of **Pc-PBBA COF** also suggested an H-aggregated structure. CH_2Cl_2 solutions of **4** fluoresce strongly with a small Stokes shift (17 nm, $\lambda_{em} = 708$ nm), typical of monomeric phthalocyanines of similar structure. The solid samples of **Pc-PBBA COF** were non-emissive, as observed for other phthalocyanine H-aggregates (see Supplementary Fig. S21). Also, these results can be understood by exciton theory[44]. We expected **4** to form non-emissive aggregates in the solid state, but found that both powders and drop-cast films of **4** fluoresced very weakly at 820 nm. We hypothesize that the four acetonide groups distort the cofacial aggregates of **4**, which results in weakly allowed emission from a dimer or aggregate of higher order. This process was not observed in the more structurally precise COF. The changes in both absorption and emission spectra of the phthalocyanine moieties observed in the COF materials strongly suggest cofacial stacking.

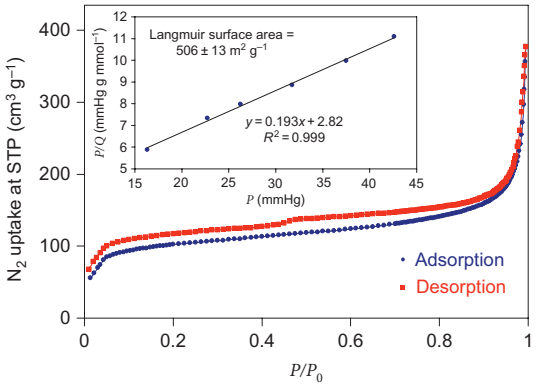

Figure 5 | Nitrogen-adsorption isotherms suggest that the Pc-PBBA COF is microporous. The isotherm indicates reversible nitrogen uptake with a small hysteresis at about $P/P_0 = 0.5$ ($P_0 = 1$ atm). The linear portion of the plot between 0.02 and 0.06 was used to calculate a Langmuir surface area of 506 $m^2\ g^{-1}$ (inset; Q = gas adsorbed per unit mass of analyte). The small phenylene spacer unit and large phthalocyanine core result in a unit cell that is only about 75% free space; even so, reasonably high surface areas were observed for this COF.

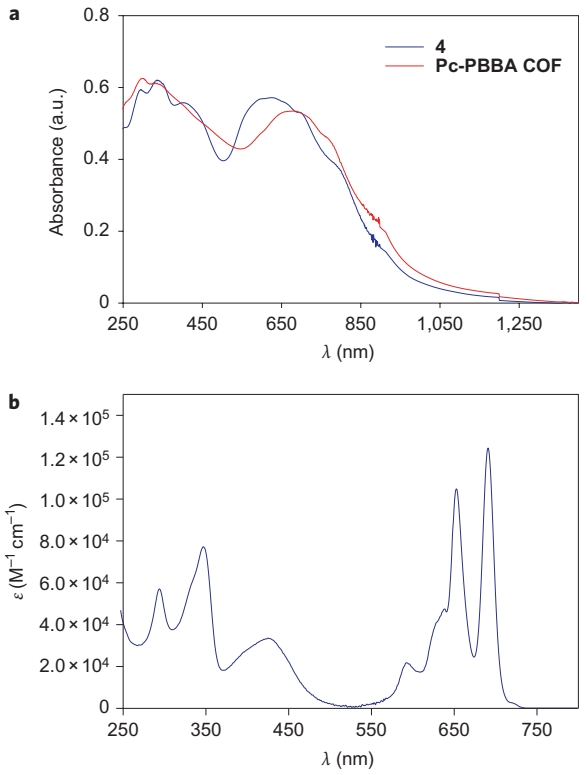

Figure 6 | Pc-PBBA COF absorbs light over a broad range of the visible and near-infrared spectral regions. a,**b** Blue shifts of the absorption maxima of phthalocyanine acetonide powder **4** (**a**, blue) and the **Pc-PBBA COF** (**a**, red) relative to CH_2Cl_2 solutions of **4** (**b**) are consistent with stacked phthalocyanines. Spectral broadening of the phthalocyanine *Q* bands results in a material that absorbs light over most of the solar spectrum.

Phthalocyanine J-aggregates (offset stacks) show red-shifted absorption spectra and are emissive[45]. Furthermore, disordered phthalocyanine-containing macroporous polymers[46] that prevent phthalocyanine aggregation show absorption and emission spectral behaviour in the solid state similar to the spectral behaviour of the solution of **4**.

In conclusion, we developed a new Lewis acid-catalysed protocol to synthesize boronate ester-linked COFs directly from acetonide-protected catechols. We expect this method to broaden greatly the scope of catechol derivatives that may be incorporated into these materials. It enabled us to prepare an eclipsed 2D COF from a synthetically convenient phthalocyanine tetra(acetonide) precursor. The synthetic availability, structural precision and robust nature of these materials make them excellent candidates for organic photovoltaic devices. The pores created by vertical stacking of the sheets present an opportunity to introduce a complementary organic semiconductor to obtain structurally precise bulk heterojunction composites, a goal we are currently pursuing.

Methods

Phthalocyanine tetra(acetonide) 4. Phthalonitrile[30] **7** (1.20 g, 5.99 mmol; see Supplementary Information) was dissolved in 1-pentanol (20 ml) and lithium metal granules (420 mg, 60 mmol) were added at room temperature with vigorous stirring. The mixture was heated to reflux (140 °C) for five hours under a nitrogen atmosphere. During this time, the reaction mixture turned very dark green. Then the mixture was cooled to room temperature, and glacial acetic acid (20 ml) added as the mixture was stirred. After 30 minutes the solution was concentrated under vacuum. The resulting green residue was dissolved in a mixture of $CHCl_3$ and MeOH (15:1, 100 ml) and washed with brine (3 × 100 ml) and H_2O (1 × 100 ml). The dark-green organic layer was dried with $MgSO_4$ and concentrated to a volume of 50 ml. The solution was triturated with 200 ml of hexane, which caused a dark green precipitate to form. This precipitate was isolated from the brown supernatant by centrifugation. The trituration and centrifugation steps were repeated to provide the phthalocyanine tetra(acetonide) **4** (620 mg, 52%) as a dark indigo-blue solid. Matrix-assisted laser desorption–ionization mass spectrometry (MALDI-MS): 802.20 (M^+). Infrared (powder, ATR): 2,990, 2,921, 2,850, 1,764, 1,716, 1,682, 1,603, 1,474, 1,447, 1,409, 1,386, 1,376, 1,250, 1,214, 1,073, 1,026, 1,002, 979, 852, 812, 785, 737, 714 cm^{-1}. Ultraviolet–visible, 2.08 μM in CH_2Cl_2, λ (nm) (log ε (M^{-1} cm^{-1})): 691 (5.09), 653 (5.02), 638 (4.68, shoulder), 592 (4.34), 425 (4.53), 347 (4.89), 294 (4.76). Ultraviolet–visible (powder, praying mantis diffuse reflection accessory (DRA)): 609, 396, 331, 289 nm. Analytically calculated for $C_{44}H_{34}N_8O_8$: C, 65.83; H, 4.27; N, 13.96. Found: C, 64.66; H, 3.91; N, 13.10. The MALDI-MS and ultraviolet–visible absorption spectra of **4** match those reported previously[47].

Pc-PBBA COF. Phthalocyanine acetonide **4** (32 mg, 0.040 mmol) and PBBA (**5**, 18.5 mg, 0.112 mmol) were loaded into a 1 dram screw-cap vial and suspended in a mixture of mesitylene and DCE (1:1, 1.5 ml). The dark-blue mixture was sonicated for 15 minutes. Boron trifluoride etherate (15 μl, 0.12 mmol) was added, and the mixture was sonicated for another 15 minutes. The dark, heterogeneous mixture was transferred to a pre-scored KIMAX-51 borosilicate glass ampoule (5 ml, body length 37 mm, outer diameter 17 mm, neck length 51 mm) and flash frozen in a liquid nitrogen bath. The ampoule neck was flame-sealed in air using a propane torch, which reduced the total length by 20–30 mm. After warming to room temperature the suspension was placed in a gravity convection oven at 120 °C for six days. The reaction was cooled to room temperature, the ampoule was broken at the scored neck and the mixture was poured onto qualitative filter paper (medium porosity) on a Hirsch filter funnel and filtered under vacuum. The resulting dark solid was washed with anhydrous CH_3CN (4 ml) and dried in air. The solid was loaded into a 1 dram screw-cap vial and suspended in anhydrous CH_3CN (3 ml) overnight, and again recovered by filtration to yield **Pc-PBBA COF** as a dark-green solid (16 mg, 48%). Infrared (powder, ATR): 3,272, 1,605, 1,523, 1,469, 1,439, 1,373, 1,328, 1,272, 1,187, 1,079, 1,018, 866, 849, 810, 739, 709, 653 cm^{-1}. PXRD (2θ (relative intensity)): 3.84° (100), 7.76° (17), 8.56° (8), 11.68° (8), 26.52° (19), 26.64° (19). Ultraviolet–visible (powder, praying mantis DRA): 671, 325, 293 nm. Analytically calculated for $(C_{11}H_5BN_2O_2)_n$: C, 63.52; H, 2.42; N, 13.47. Found: C, 53.54; H, 2.41; N, 11.02. Elemental analysis of boronate COFs typically give lower carbon values to those from the formation of non-combustible boron carbide by-products[13]. We also anticipate a similar formation of boron nitride by-products, which lower the nitrogen value. The presence of boron was confirmed by a characteristic B 1*s* peak in the X-ray photoelectron spectrum with a binding energy of 192.839 eV and an abundance of 4.66% (calculated: 5.33% excluding hydrogens).

Received 14 January 2010; accepted 6 May 2010; published online 20 June 2010

References

1. Anthony, J. E. Functionalized acenes and heteroacenes for organic electronics. *Chem. Rev.* **106,** 5028–5048 (2006).
2. Park, J.-S. *et al.* Flexible full color organic light-emitting diode display on polyimide plastic substrate driven by amorphous indium gallium zinc oxide thin-film transistors. *Appl. Phys. Lett.* **95,** 013503 (2009).
3. Subramanian, V. *et al.* Progress toward development of all-printed RFID tags: materials, processes, and devices. *Proc. IEEE* **93,** 1330–1338 (2005).
4. Müllen, K. & Scherf, U. *Organic Light Emitting Devices: Synthesis, Properties and Applications* (Wiley-VCH, 2006).
5. Thomas, S. W., Joly, G. D. & Swager, T. M. Chemical sensors based on amplifying fluorescent conjugated polymers. *Chem. Rev.* **107,** 1339–1386 (2007).
6. Briseno, A. L. *et al.* Patterning organic single-crystal transistor arrays. *Nature* **444,** 913–917 (2006).
7. Brabec, C. J. D., Parisi, J. & Sariciftci, N. S. *Organic Photovoltaics Concepts and Realization* (Springer-Verlag, 2003).
8. Lloyd, M. T., Anthony, J. E. & Malliaras, G. G. Photovoltaics from soluble small molecules. *Mater. Today* **10,** 34–41 (2007).
9. Coropceanu, V. *et al.* Charge transport in organic semiconductors. *Chem. Rev.* **107,** 926–952 (2007).
10. Anthony, J. E., Brooks, J. S., Eaton, D. L. & Parkin, S. R. Functionalized pentacene: improved electronic properties from control of solid-state order. *J. Am. Chem. Soc.* **123,** 9482–9483 (2001).
11. Mas-Torrent, M. *et al.* Correlation between crystal structure and mobility in organic field-effect transistors based on single crystals of tetrathiafulvalene derivatives. *J. Am. Chem. Soc.* **126,** 8546–8553 (2004).
12. Desiraju, G. R. Cryptic crystallography. *Nature Mater.* **1,** 77–79 (2002).
13. Côté, A. P. *et al.* Porous, crystalline, covalent organic frameworks. *Science* **310,** 1166–1170 (2005).
14. Tilford, R. W., Gemmill, W. R., zur Loye, H. C. & Lavigne, J. J. Facile synthesis of a highly crystalline, covalently linked porous boronate network. *Chem. Mater.* **18,** 5296–5301 (2006).
15. Kuhn, P., Antonietti, M. & Thomas, A. Porous, covalent triazine-based frameworks prepared by ionothermal synthesis. *Angew. Chem. Int. Ed.* **47,** 3450–3453 (2008).

16. Furukawa, H. & Yaghi, O. M. Storage of hydrogen, methane, and carbon dioxide in highly porous covalent organic frameworks for clean energy applications. *J. Am. Chem. Soc.* **131,** 8875–8883 (2009).
17. Wan, S., Guo, J., Kim, J., Ihee, H. & Jiang, D. L. A belt-shaped, blue luminescent, and semiconducting covalent organic framework. *Angew. Chem. Int. Ed.* **47,** 8826–8830 (2008).
18. Wan, S., Guo, J., Kim, J., Ihee, H. & Jiang, D. L. A photoconductive covalent organic framework: self-condensed arene cubes composed of eclipsed 2D polypyrene sheets for photocurrent generation. *Angew. Chem. Int. Ed.* **48,** 5439–5442 (2009).
19. Uribe-Romo, F. J. *et al.* A crystalline imine-linked 3-D porous covalent organic framework. *J. Am. Chem. Soc.* **131,** 4570–4571 (2009).
20. Hunt, J. R., Doonan, C. J., LeVangie, J. D., Côté, A. P. & Yaghi, O. M. Reticular synthesis of covalent organic borosilicate frameworks. *J. Am. Chem. Soc.* **130,** 11872–11873 (2008).
21. Tilford, R. W., Mugavero, S. J., Pellechia, P. J. & Lavigne, J. J. Tailoring microporosity in covalent organic frameworks. *Adv. Mater.* **20,** 2741–2748 (2008).
22. Tong, X., Bailey-Salzman, R. F., Wei, G. & Forrest, S. R. Inverted small molecule organic photovoltaic cells on reflective substrates. *Appl. Phys. Lett.* **93,** 173304 (2008).
23. Pfuetzner, S., Meiss, J., Petrich, A., Riede, M. & Leo, K. Thick C_{60}:ZnPc bulk heterojunction solar cells with improved performance by film deposition on heated substrates. *Appl. Phys. Lett.* **94,** 253303 (2009).
24. Reddy, P. Y. *et al.* Efficient sensitization of nanocrystalline TiO_2 films by a near-IR-absorbing unsymmetrical zinc phthalocyanine. *Angew. Chem. Int. Ed.* **46,** 373–376 (2007).
25. Moreira, L. M. *et al.* Photodynamic therapy: porphyrins and phthalocyanines as photosensitizers. *Aust. J. Chem.* **61,** 741–754 (2008).
26. de la Torre, G., Vaquez, P., Agullo-Lopez, F. & Torres, T. Role of structural factors in the nonlinear optical properties of phthalocyanines and related compounds. *Chem. Rev.* **104,** 3723–3750 (2004).
27. Kadish, K. M., Smith, K. M. & Guilard, R. *The Porphyrin Handbook* Vol. 15–20 (Academic, 2002).
28. Seltzman, H. H., Fleming, D. N., Hawkins, G. D. & Carroll, F. I. Facile synthesis and stabilization of 2-arachidonylglycerol via its 1,3-phenylboronate ester. *Tetrahedron Lett.* **41,** 3589–3592 (2000).
29. Côté, A. P., El-Kaderi, H. M., Furukawa, H., Hunt, J. R. & Yaghi, O. M. Reticular synthesis of microporous and mesoporous 2D covalent organic frameworks. *J. Am. Chem. Soc.* **129,** 12914–12915 (2007).
30. Baugh, S. D. P., Yang, Z. W., Leung, D. K., Wilson, D. M. & Breslow, R. Cyclodextrin dimers as cleavable carriers of photodynamic sensitizers. *J. Am. Chem. Soc.* **123,** 12488–12494 (2001).
31. Vanderpol, J. F. *et al.* A polymer with the mesomorphic order of liquid–crystalline phthalocyanines. *Macromolecules* **23,** 155–162 (1990).
32. Ruf, M., Lawrence, A. M., Noll, B. C. & Pierpont, C. G. Silicon and zinc coordination to peripheral catechol sites of (2,3,9,10,16,17,23,24-octahydroxyphthalocyaninato)nickel(II). Phthalocyanine coordination chemistry at the edge. *Inorg. Chem.* **37,** 1992–1999 (1998).
33. Materials Studio Release Notes v.4.4 (Accelrys Software, San Diego, 2008).
34. Sichel, E. K., Miller, R. E., Abrahams, M. S. & Buiocchi, C. J. Heat capacity and thermal conductivity of hexagonal pyrolytic boron nitride. *Phys. Rev. B* **13,** 4607–4611 (1976).
35. Liang, J. & Shimizu, G. K. H. Crystalline zinc diphosphonate metal–organic framework with three-dimensional microporosity. *Inorg. Chem. Commun.* **46,** 10449–10451 (2007).
36. Thallapally, P. K. *et al.* Carbon dioxide capture in a self-assembled organic nanochannels. *Chem. Mater.* **19,** 3355–3357 (2007).
37. Mulfort, K. L., Wilson, T. M., Wasielewski, M. R. & Hupp, J. T. Framework reduction and alkali-metal doping of a triply catenating metal–organic framework enhances and then diminishes H_2 uptake. *Langmuir* **25,** 503–508 (2009).
38. Svec, F., Germain, J. & Fréchet, J. M. J. Nanoporous polymers for hydrogen storage. *Small* **5,** 1098–1111 (2009).
39. Yuan, S. W., Kirklin, S., Dorney, B., Liu, D. J. & Yu, L. P. Nanoporous polymers containing stereocontorted cores for hydrogen storage. *Macromolecules* **42,** 1554–1559 (2009).
40. Noro, S. *et al.* Selective gas adsorption in one-dimensional, flexible Cu-II coordination polymers with polar units. *Chem. Mater.* **21,** 3346–3355 (2009).
41. Barrett, E. P., Joyner, L. G. & Halenda, P. P. The determination of pore volume and area distributions in porous substances. I. Computations from nitrogen isotherms. *J. Am. Chem. Soc.* **73,** 373–380 (2002).
42. Orilall, M. C. *et al.* One-pot synthesis of platinum-based nanoparticles incorporated into mesoporous niobium oxide–carbon composites for fuel cell electrodes. *J. Am. Chem. Soc.* **131,** 9389–9395 (2009).
43. Tant, J. *et al.* Liquid crystalline metal-free phthalocyanines designed for charge and exciton transport. *J. Phys. Chem. B* **109,** 20315–20323 (2005).
44. Cornil, J., dos Santos, D. A., Crispin, X., Silbey, R. & Brédas, J. L. Influence of interchain interactions on the absorption and luminescence of conjugated oligomers and polymers: a quantum-chemical characterization. *J. Am. Chem. Soc.* **120,** 1289–1299 (1998).
45. Huang, X. *et al.* Self-assembled nanowire networks of aryloxy zinc phthalocyanines based on Zn–O coordination. *Langmuir* **23,** 5167–5172 (2007).
46. McKeown, N. B., Makhseed, S. & Budd, P. M. Phthalocyanine-based nanoporous network polymers. *Chem. Commun.* 2780–2781 (2002).
47. Ivanov, A. V., Svinareva, P. A., Zhukov, I. V. Tomilova, L. G. & Zefirov, N. S. New phthalocyanine complexes based on 4,5-isopropylidenedioxyphthalonitrile. *Russ. Chem. Bull. Int. Ed.* **52,** 1562–1566 (2003).

Acknowledgements

This research was supported by start-up funds provided by Cornell University and the National Science Foundation (NSF)-funded Centers for Chemical Innovation Phase I Center for Molecular Interfacing (CHE-0847926). We also made use of the Cornell Center for Materials Research facilities with support from the NSF Materials Research Science and Engineering Centers program (DMR-0520404). E.L.S. acknowledges the award of the American Competitiveness in Chemistry postdoctoral fellowship from the NSF (CHE-0936988). We thank H. Sai and N. Hoepker for instrument assistance and A. Côté and A. Beeby for discussions.

Author contributions

Both authors conceived the project, performed and interpreted the results of the experiments and wrote the manuscript.

Additional information

The authors declare no competing financial interests. Supplementary information and chemical compound information accompany this paper at www.nature.com/naturechemistry. Reprints and permission information is available online at http://npg.nature.com/reprintsandpermissions/. Correspondence and requests for materials should be addressed to W.R.D.